

Food & Function

Linking the chemistry and physics of food with health and nutrition

Accepted Manuscript

This article can be cited before page numbers have been issued, to do this please use: M. Albertuni, M. Torrecillas-Lopez, T. Gonzalez-de la Rosa, L. Barrera-Chamorro, E. Marquez-Paradas, J. L. del-Rio-Vazquez, M. D. Navarro-Hortal, C. Claro and S. Montserrat-de la Paz, *Food Funct.*, 2026, DOI: 10.1039/D6FO00279J.



This is an Accepted Manuscript, which has been through the Royal Society of Chemistry peer review process and has been accepted for publication.

Accepted Manuscripts are published online shortly after acceptance, before technical editing, formatting and proof reading. Using this free service, authors can make their results available to the community, in citable form, before we publish the edited article. We will replace this Accepted Manuscript with the edited and formatted Advance Article as soon as it is available.

You can find more information about Accepted Manuscripts in the [Information for Authors](#).

Please note that technical editing may introduce minor changes to the text and/or graphics, which may alter content. The journal's standard [Terms & Conditions](#) and the [Ethical guidelines](#) still apply. In no event shall the Royal Society of Chemistry be held responsible for any errors or omissions in this Accepted Manuscript or any consequences arising from the use of any information it contains.

1 **Oleic and omega-3 fatty acids buffer neuroinflammation in a scopolamine model with** Open Access Article Online
DOI: 10.1039/D6FO00279J
2 **Alzheimer's-like features via target-level interactions**

3 Marlua Albertuni¹, Maria Torrecillas-Lopez^{1,2}, Teresa Gonzalez-de la Rosa^{1,2}, Luna Barrera-
4 Chamorro^{1,2}, Elvira Marquez-Paradas^{1,2}, Jose L. del Rio-Vazquez¹, Maria D. Navarro-
5 Hortal¹, Carmen M. Claro-Cala^{2,3,*}, Sergio Montserrat-de la Paz^{1,2}

6 ¹ Department of Medical Biochemistry, Molecular Biology and Immunology, School of
7 Medicine, University of Seville. Av. Sanchez Pizjuan s/n, 41009 Seville, Spain.

8 ² Instituto de Biomedicina de Sevilla, IBiS/Hospital Universitario Virgen del
9 Rocio/CSIC/Universidad de Sevilla, Seville, 41013, Spain.

10 ³ Department of Pharmacology, Pediatrics, and Radiology, School of Medicine, University of
11 Seville, 41009 Seville, Spain.

12

13 **Corresponding author:**

14 Prof. Carmen M. Claro-Cala

15 Department of Pharmacology, Pediatrics, and Radiology, School of Medicine, University of
16 Seville, 41009 Seville, Spain.

17 E-mail: cmclaro@us.es

18

19 **Running title:** Oleic and omega-3 fats buffer neuroinflammation.

20

21

22

23

24

25

26

27

28



29 **ABSTRACT**View Article Online
DOI: 10.1039/D6FO00279J

30 Diet quality, beyond total fat, may shape brain immune tone in Alzheimer's-relevant contexts.
31 We examined whether the fatty acid profile and food matrix of high-fat diets (HFD) modulate
32 hippocampal neuroinflammation *in vivo* and explored target-level mechanisms with molecular
33 docking. Male B6129SF2/J mice received standard diet (SD) or HFD enriched in extra-virgin
34 olive oil (EVOO), refined olive oil (ROO), refined palm oil (RPO), or ω 3 long-chain
35 polyunsaturated fatty acids (ω 3-LCPUFA). During the final week, scopolamine induced acute
36 cholinergic dysfunction. Neuroinflammation was assessed in the dentate gyrus by IHC (Iba-1,
37 COX-2, TNF- α) and by IF of astrocytes (GFAP intensity and morphology). Docking evaluated
38 interactions of oleic and palmitic acids, EPA, and DHA with AChE, COX-2, BACE1, and
39 TREM2. All HFDs attenuated scopolamine-evoked increases in Iba-1, COX-2 and TNF- α
40 versus SD-scopolamine, with limited separation among lipid classes under this acute stressor.
41 By contrast, astroglial readouts showed a clear hierarchy: EVOO-HFD produced the lowest
42 GFAP signal and the most ramified morphology, followed closely by ω 3-LCPUFA, with ROO
43 intermediate and SFA least favourable. Docking supported a mechanistic scaffold: EPA/DHA
44 displayed stronger predicted engagement than oleate/palmitate at COX-2 and BACE1, while
45 long-chain fatty acids populated the AChE peripheral site and a lipid/apoE-responsive surface
46 on TREM2. In conclusion, PUFA-rich feeding, and notably the EVOO matrix preferentially
47 buffer hippocampal neuroinflammation in a scopolamine-induced Alzheimer's-like model.
48 These findings support a composition, binding, and function framework and strengthen the
49 translational rationale for precision nutrition strategies prioritizing ω 3-LCPUFA and high-
50 quality olive oils.

51 **Keywords:** Alzheimer's disease; dietary fatty acids; omega-3 long-chain PUFA; extra-virgin
52 olive oil; neuroinflammation; astrocytes; microglia; BACE1.

53

54

55

56

57

58

59

60

61

62



63

64 **1. INTRODUCTION**

65 Alzheimer's disease (AD) is a multifactorial neurodegenerative disorder in which amyloid- β
66 (A β) deposition and tau pathology coexist with a persistent, maladaptive neuroinflammatory
67 milieu orchestrated by microglia and astrocytes.¹ Beyond the classical proteinopathies,
68 disturbances in lipid handling and membrane composition are increasingly recognised as
69 upstream drivers of immune dysregulation and synaptic failure, placing brain lipid metabolism,
70 and its dietary determinants, at the centre of disease biology.^{2,3}

71 Diet quality, particularly the fatty acid profile and the presence of bioactive phenolics from
72 olive products, has been consistently linked to brain health.^{4,5} Adherence to Mediterranean-style
73 dietary patterns, characterised by extra-virgin olive oil (EVOO) as the principal fat source,
74 associates with more favourable cognitive trajectories, whereas Western-type fat patterns
75 enriched in saturated fatty acids (SFAs) align with neuroinflammatory phenotypes.^{6,7}
76 Mechanistically, EVOO phenolics and the broader food matrix modulate oxidative and
77 inflammatory pathways and engage the gut-brain axis, providing a plausible route by which
78 specific foods can reshape neuroimmune tone.⁸ Among dietary fats, omega-3 long-chain
79 polyunsaturated fatty acids (ω 3-LCPUFAs) such as docosahexaenoic acid (DHA) and
80 eicosapentaenoic acid (EPA) exert neuroprotective actions that include tuning microglial
81 phenotype and function.⁹ Experimental and translational evidence indicates that ω 3-LCPUFAs
82 availability shapes microglial lipid metabolism and phagocytic programmes, whereas deficiency
83 states exacerbate synaptic pruning and behavioural impairment.^{10,11} These data converge on the
84 principle that brain-resident immunity is exquisitely sensitive to systemic lipid inputs. In
85 parallel, olive-derived phenolics interact with AD-relevant pathways.¹² Oleocanthal enhances
86 A β clearance and reduces aggregation toxicity, supporting a food-borne small-molecule
87 rationale alongside macronutrient effects, while broader EVOO phenolic profiles display
88 antioxidant and anti-inflammatory activities pertinent to neurodegeneration.^{13,14} Together, these
89 strands point to complementary, multi-tiered benefits of both fatty acid quality and phenolic
90 biochemistry within olive-centred dietary patterns. At the same time, not all fatty acids are
91 equal. SFAs such as palmitic acid have been reported to promote inflammatory signalling,
92 including proposed TLR4/MD-2 interactions, however, this remains debated and may reflect
93 broader lipid-induced immunometabolic reprogramming rather than direct receptor ligation.¹⁵⁻¹⁷
94 These mixed findings underscore the need to resolve lipid-protein interaction landscapes
95 relevant to neuroinflammation. Molecular docking therefore provides a tractable first pass to
96 map how major dietary fatty acids might engage AD- and inflammation-related targets,
97 complementing *in vivo* models that test causal links between dietary fat quality and
98 neuroimmune outcomes.¹⁸



99 Here, building on this framework, we test whether dietary fat quality modulates
100 neuroinflammatory readouts in a murine model of AD-like cholinergic dysfunction and, in
101 parallel, we perform *in silico* docking of the major fatty acids from each diet against canonical
102 AD/neuroinflammatory targets to propose mechanistic links between nutrient composition and
103 neuroimmune signalling. This integrated strategy is designed to connect composition, binding,
104 and function, thereby strengthening the translational rationale for precision nutrition approaches
105 in Alzheimer's-relevant contexts.

106 2. MATERIALS AND METHODS

107 2.1. Materials

108 Unless otherwise specified, analytical-grade reagents were used. Dietary lipid sources for diet
109 preparation and lipid profiling were extra-virgin olive oil (EVOO) and refined olive oil (ROO;
110 Ybarra, Seville, Spain), refined palm oil (RPO; Lipsa, Barcelona, Spain), and fish-oil capsules
111 (Omacor®, Seville, Spain). Primary antibodies were anti-Iba-1 (rabbit, 1:500; Santa Cruz,
112 Dallas, TX, USA, sc-98468), anti-COX-2 (goat, 1:200; Santa Cruz, sc-1747), anti-TNF- α
113 (mouse, 1:100; Santa Cruz, sc-133192), anti-GFAP (rabbit, 1:500; Dako, Glostrup, Denmark,
114 Z0334). Secondary antibodies (Vector Laboratories, Newark, CA, USA) were anti-rabbit IgG
115 (HRP, 1:1000; BA-1000), anti-goat IgG (HRP, 1:500; BA-5000), anti-mouse IgG (HRP, 1:500;
116 BA-2000). For immunofluorescence (IF), FITC-conjugated anti-rabbit IgG was used (1:500;
117 Jackson, West Grove, PA, USA, 711-095-152). Chromogenic detection employed DAB (Sigma-
118 Aldrich, Darmstadt, Germany) and the ABC kit (Vector, PK-6100). Nuclear counterstaining
119 used Hoechst/DAPI and neurodegeneration was assessed with the Fluoro-Jade C kit (FJC,
120 Biosensis, Thebarton, SA, Australia), following manufacturer instructions. Imaging was
121 performed on an Olympus BX41 microscope with an XM10 camera (Olympus, Tokyo, Japan)
122 and on a Zeiss LSM 7 DUO confocal system (Carl Zeiss, Oberkochen, Germany); image
123 analysis was conducted in ImageJ (NIH, Bethesda, MD, USA) under identical acquisition
124 settings across groups.

125 2.2. Fatty acid profiling of oils (GC-FID)

126 Fatty-acid methyl esters (FAMES) were analysed on a GC 6890N equipped with a flame-
127 ionization detector (FID, Agilent Technologies, Santa Clara, CA, USA) using an HP-88
128 capillary column (100 m \times 0.25 mm i.d., 0.2 μ m film; Agilent J&W, Folsom, CA, USA).¹⁹ The
129 carrier gas was hydrogen at 2 mL min⁻¹ (constant-flow mode). The oven programme was: 100
130 °C (start), ramp 3 °C min⁻¹ to 158 °C, then 1.5 °C min⁻¹ to 190 °C (hold 15 min), then 2 °C
131 min⁻¹ to 200 °C, then 10 °C min⁻¹ to 240 °C (hold 10 min). Injector: 300 °C; detector: 320 °C.
132 Peaks were identified against a certified FAME standard mixture, and results are expressed as g
133 per 100 g of total fatty acids (Supplementary Material-Table S1).



134 2.3. Animals, ethics, diets, and experimental design

135 Male B6129SF2/J mice (5–8 weeks; The Jackson Laboratory, Bar Harbor, ME, USA, stock
136 101045) were housed (2–4 per cage) under a 12 h light/dark cycle at 21 ± 2 °C and 50–50%
137 relative humidity, with *ad libitum* access to water and chow and standard environmental
138 enrichment. All procedures complied with EU Directive 2010/63 and Spanish RD 53/2013 and
139 were approved by the Animal Research Ethics Committee of the University of Seville and the
140 Andalusian Committee for Animal Experimentation (approval 26/08/2020/101). After 1 week of
141 acclimatization, mice were randomized into five dietary groups ($n = 8–10$ per group): (i) SD
142 (standard diet); (ii) HFD-MUFA (SD supplemented with 47% EVOO); (iii) HFD-rMUFA (47%
143 ROO); (iv) HFD-SFA (47% RPO); and (v) HFD- ω 3-LCPUFA (32% ROO + 15% fish oil). The
144 supplementation level (47%) was selected to convert the standard chow (\approx 13% energy from fat)
145 into a high-fat dietary background providing \sim 60% of total energy from fat, thereby creating an
146 obesogenic/metabolic-stress context in which fat quality (source and fatty-acid profile) could be
147 tested while keeping the overall fat-derived energy comparable across high-fat groups (13%
148 from chow + 47% from supplemented oils). Thus, the study design was isocaloric/isofat across
149 HFD groups, differing primarily in the lipid source and fatty-acid composition. For the HFD-
150 ω 3-LCPUFA group, the total supplemented oil was kept constant (47%) to maintain comparable
151 fat-derived energy; however, 15% of the supplemented lipid was provided as fish oil to enrich
152 the diet in EPA/DHA, while the remaining 32% ROO served as a MUFA background/carrier to
153 preserve diet comparability and feasibility and to avoid using fish oil as the sole supplemental
154 fat (which can be more prone to oxidation and may impact palatability and intake). Body weight
155 and food intake were recorded weekly. During the final week, all groups, except half of the SD
156 group, received scopolamine hydrobromide (1 mg kg^{-1} , i.p.; three injections on alternating days
157 over 5 days) to induce Alzheimer's-like cholinergic dysfunction;²⁰ the remaining SD subgroup
158 received vehicle and served as an intra-group control. At week 10, animals were anaesthetised
159 (ketamine 100 mg kg^{-1} + xylazine 10 mg kg^{-1} , i.p.) and euthanised; brains were collected for
160 histological analyses. Outcome assessment and image quantification were performed blinded to
161 group allocation. A schematic of the experimental timeline and group allocation is shown in
162 **Figure 1.**

163

164

165

166

167



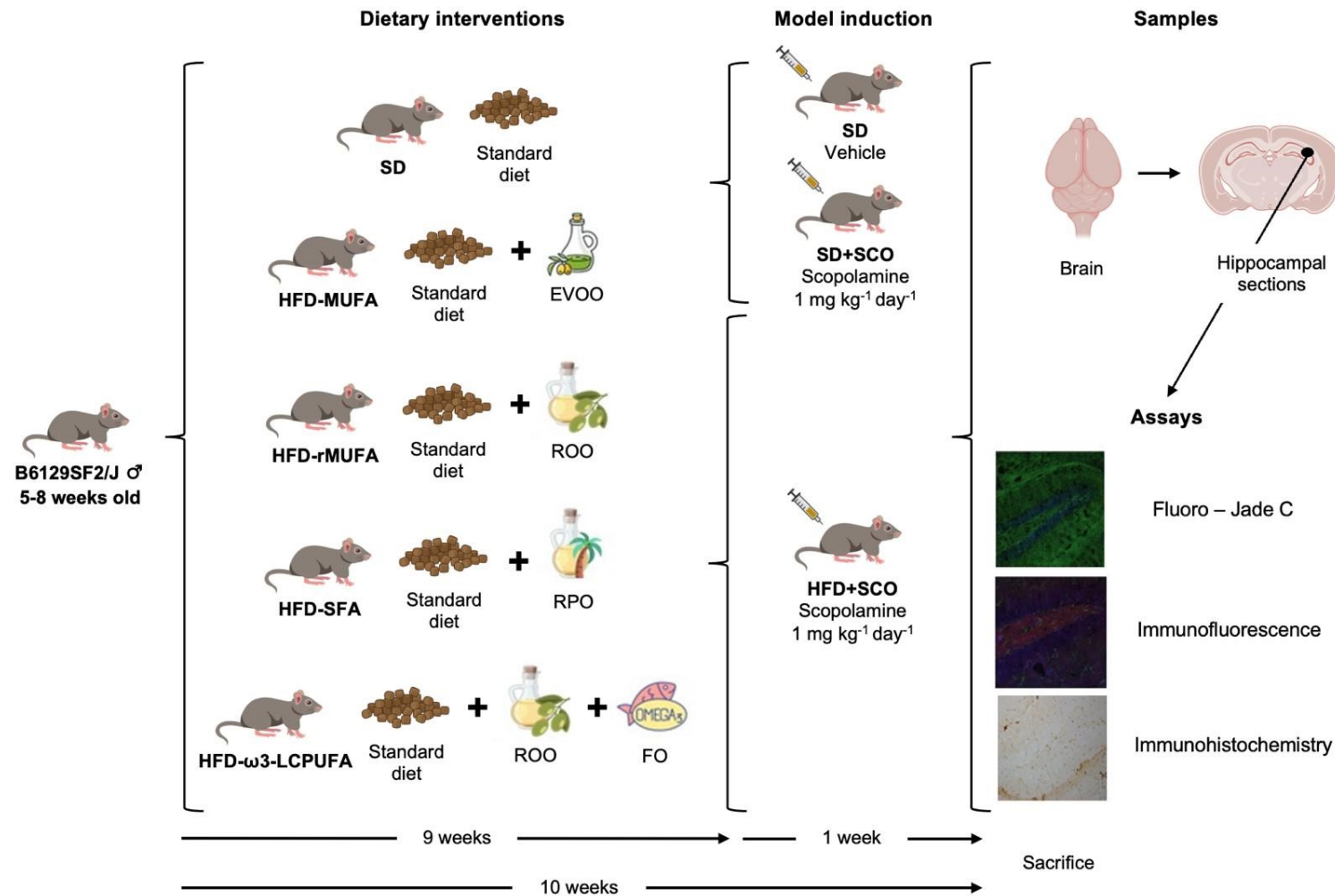


Figure 1. Schematic of the 10-week feeding intervention and scopolamine challenge. After a 1-week acclimatization, male B6129SF2/J mice were randomized to standard diet (SD), HFD-MUFA (extra-virgin olive oil, EVOO), HFD-rMUFA (refined olive oil, ROO), HFD-SFA (refined palm oil, RPO), or HFD- ω 3-LCPUFA (ROO + fish oil, FO). Scopolamine (1 mg kg^{-1} , i.p.) was administered on three alternating days during the final week to all groups except one SD subgroup (vehicle control). Body weight and food intake were recorded weekly. At week 10, brains were collected for IHC/IF and Fluoro-Jade C analyses. All outcome assessments and image quantifications were performed blinded to group.

185 2.4. Tissue processing and histological analyses

186 Brains were immersion-fixed in 10% paraformaldehyde for 24 h, cryoprotected in 15% and then
187 30% sucrose, embedded in OCT, and stored at -80°C . Coronal sections (hemisphere, $20\ \mu\text{m}$)
188 were cut at -20°C and collected in PBS/glycerol (50%) for downstream immunohistochemistry
189 (IHC), IF, or FJC staining. For IHC, hippocampal sections were washed in PBS, endogenous
190 peroxidase was quenched with H_2O_2 , and non-specific binding was blocked with 10% FBS.
191 Sections were incubated 24 h at 4°C with primary antibodies (Iba-1, 1:500; COX-2, 1:200;
192 TNF- α , 1:100) diluted in PBS-T + 3% FBS, washed, and incubated with the corresponding
193 HRP-conjugated secondary antibodies (anti-rabbit 1:1000 for Iba-1; anti-goat 1:500 for COX-2;
194 anti-mouse 1:500 for TNF- α). Signal was developed using ABC and DAB; sections were
195 dehydrated, cleared, mounted with DPX, and imaged under identical acquisition settings across
196 groups. For IF (astroglial markers), sections were permeabilised in PBS-T (1%), blocked with
197 BSA (5%), and incubated overnight at 4°C with anti-GFAP (1:500) in PBS-T + 1% BSA. After
198 washes, sections were incubated for 1 h at room temperature in the dark with FITC-conjugated
199 anti-rabbit IgG (1:500); Hoechst/DAPI was added during the last 5 min for nuclear counterstain.
200 Sections were mounted and imaged by confocal microscopy. FJC staining to assess
201 neurodegeneration followed the manufacturer's protocol: ethanol/NaOH pre-treatment, KMnO_4
202 background suppression, FJC/DAPI staining, dehydration, mounting, and confocal imaging with
203 uniform settings. Image quantification was performed in ImageJ with constant thresholds and
204 blinded analysis. For IHC, positively stained area or integrated density for Iba-1, COX-2, and
205 TNF- α was quantified in anatomically matched hippocampal regions (three sections per mouse).
206 For IF-GFAP, integrated density, circularity ($4\pi \cdot \text{area}/\text{perimeter}^2$), and aspect ratio (major
207 axis/minor axis) were computed from binarised images to capture astrocyte reactivity and
208 morphology. For glial analyses, brain sections were selected using the same anatomical criteria
209 across animals (comparable rostro-caudal levels) and processed in parallel to minimize batch
210 effects. Images were acquired under identical microscope settings for all groups
211 (exposure/gain/laser power kept constant within each marker). For each animal, multiple non-
212 overlapping fields of view were recorded per section and across sections within the region(s) of
213 interest, and the mean value per animal was used for all downstream statistical analyses (animal
214 as the experimental unit).

215 2.5. Molecular docking of major dietary fatty acids

216 We assessed putative interactions between prevalent dietary fatty acids and AD-related proteins
217 using a standardised, structure-based docking workflow. Oleic acid (PubChem CID 445639),
218 palmitic acid (985), EPA (445580), and DHA (5281168) were downloaded as SDF files,
219 imported into UCSF Chimera v1.16, protonated at pH 7.4, assigned Gasteiger charges and



220 energy-minimised; all ligand torsions were left flexible and PDBQT files were generated with
221 MGLTools/AutoDockTools v1.5.7. Receptors were the TREM2 ectodomain (PDB 5UD7),
222 acetylcholinesterase (AChE, 5DTI), COX-2 (PDB 1DDX), and β -secretase 1 (BACE1, 1FKN),
223 retrieved from the RCSB PDB, inspected for missing residues/alternate conformers, stripped of
224 co-ligands/ions/waters, protonated at pH 7.4, locally minimised in binding pockets when
225 needed, and saved as PDBQT. Binding sites and grid maps were generated with AGFR (ADFR
226 Suite v1.0): for AChE, COX-2, and BACE1, grids were centred on the orthosteric cavities
227 defined by their co-crystallized ligands; for TREM2, the grid encompassed the ApoE-interacting
228 surface previously implicated in agonist responses.²¹ Grid boxes covered the pocket plus ~4–6
229 Å margins (grid spacing 0.375 Å). Docking was performed with AutoDockFR (ADFR Suite
230 v1.0; AD4 scoring) under high-search settings (100 GA runs/ligand, population 200, $\sim 2.5 \times 10^6$
231 evaluations/run; random seed 12345). Receptors were rigid by default and a sensitivity check
232 allowing limited side-chain flexibility of pocket hydrophobes. Quality control included
233 redocking accepting RMSD ≤ 2.0 Å versus crystallographic poses. The best pose per ligand-
234 target pair was selected by predicted binding free energy (ΔG , kcal mol⁻¹) and chemical
235 plausibility and analysed in BIOVIA Discovery Studio Visualizer v21 to generate 2D/3D
236 interaction summaries.

237 2.6. Statistical analysis

238 Data are reported as mean \pm SD, with the animal as the unit of analysis ($n = 8-10$ per group).
239 Group comparisons were performed by one-way ANOVA followed by Tukey's post hoc test.
240 Statistical significance was set at $p < 0.05$. We report exact p -values (to four decimals, or " $p <$
241 0.001"). Analyses and plots were generated in GraphPad Prism v10.4.2 (GraphPad Software,
242 San Diego, CA, USA). All quantifications were conducted blinded to group allocation. The
243 animal was considered the independent biological replicate. Although multiple sections and
244 fields of view were analysed per animal, these measurements were used solely to obtain a robust
245 animal-level mean; they were not treated as independent observations (i.e., no
246 pseudoreplication). Accordingly, all statistical comparisons were performed using animal-level
247 summary values.

248 3. RESULTS AND DISCUSSION

249 3.1. Dietary fat quality diverges body weight trajectories and modulates acute 250 neurodegeneration

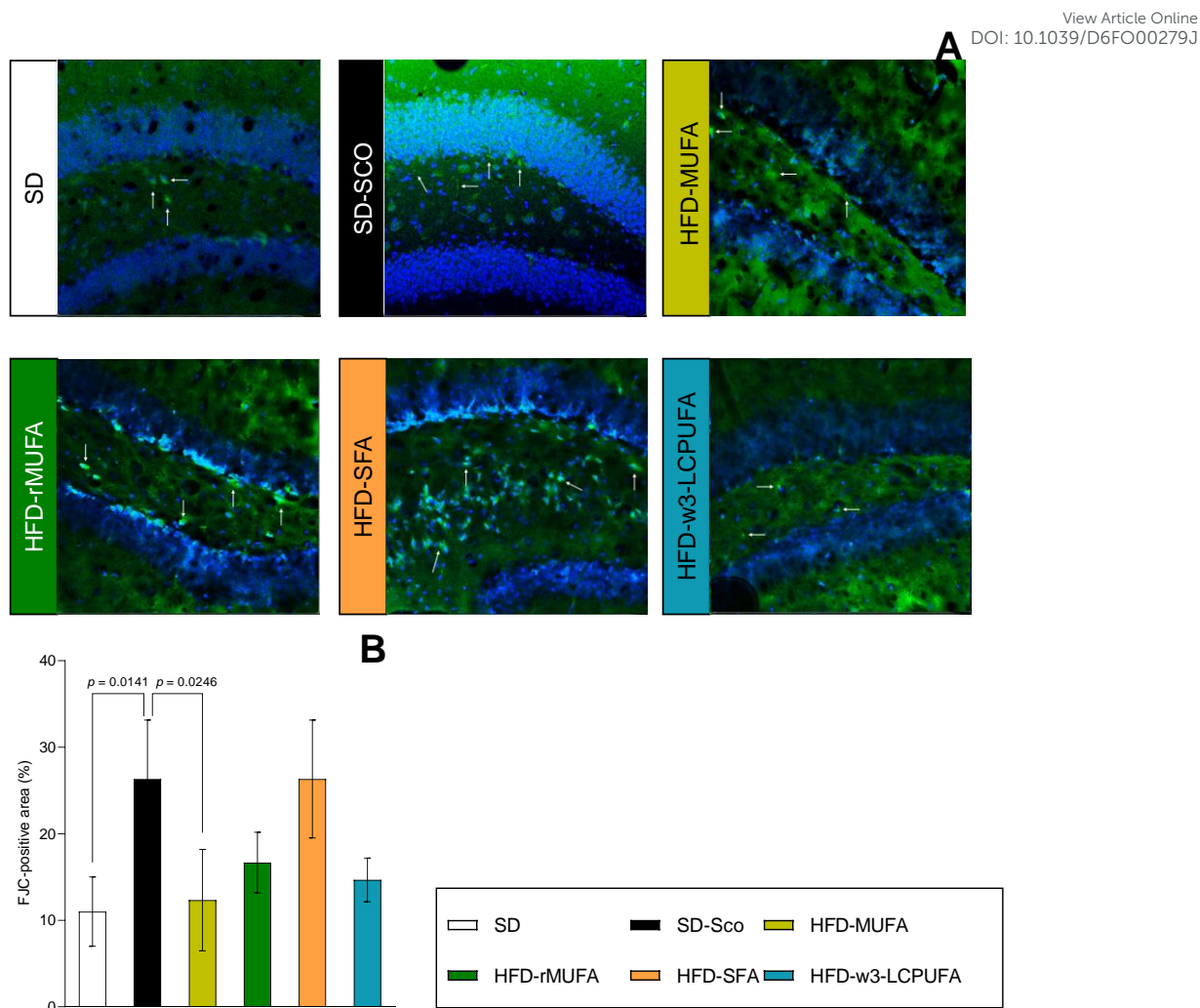
251 Across the 10-week intervention, body mass diverged as a function of fat quality
252 (Supplementary Material - Figure S1). The HFD-SFA produced the largest gain ($\approx >30\%$),
253 HFD-rMUFA an intermediate profile ($\approx 25\%$), whereas the HFD- $\omega 3$ -LCPUFA blunted weight
254 gain toward standard chow values ($\approx 11\%$; $p = 0.0412$, HFD- $\omega 3$ -LCPUFA vs HFD-SFA). HFD-



255 MUFA (EVOO) tended to attenuate accrual versus refined MUFA despite broadly similar fatty
256 acid classes, consistent with matrix/phenolic co-factors lost upon refining. Although several
257 contrasts did not reach significance, the directionality supports a role for processing and matrix,
258 not only fatty acid class, in energy balance. During the scopolamine week, HFD groups showed
259 partial weight recovery, whereas SD-Sco displayed a more persistent loss, suggesting short-term
260 metabolic buffering under acute cholinergic stress. This systemic context is relevant because
261 energetic status, adipokines, and steroid milieu can shape neurodegenerative susceptibility.

262 FJC staining in dentate gyrus revealed a diet-sensitive neurodegenerative response to
263 scopolamine (**Figure 2**). SD-Sco displayed higher FJC-positive signal than SD ($p = 0.0141$),
264 indicating increased neuronal vulnerability under acute cholinergic blockade. High-fat feeding
265 modulated this response with a clear quality hierarchy: HFD-MUFA (EVOO) exhibited the
266 lowest FJC burden among HFDs ($p = 0.0246$ vs. SD-Sco), HFD- ω 3-LCPUFA tended similarly
267 low, HFD-rMUFA was intermediate, and HFD-SFA trended highest. These patterns are
268 consistent with the hypothesis that PUFA richness and the EVOO matrix, which adds bioactive
269 phenolics absent in ROO, confer resilience to acute neurodegenerative stress, whereas an SFA-
270 biased milieu is less favourable.⁶ Several non-exclusive mechanisms may account for these
271 differences: biophysical membrane effects, where ω 3 chains enhance fluidity and may reduce
272 susceptibility to calcium dysregulation and excitotoxic cascades;^{22,23} redox/inflammatory
273 buffering via endogenous lipid mediators derived from ω 3 substrates and phenolic antioxidants
274 present in EVOO;²⁴ and metabolic preconditioning, whereby differences in weight trajectory
275 and systemic milieu (e.g., adipokines, glucocorticoids) alter the brain's threshold to acute
276 injury.²⁵ Accordingly, the ω 3-LCPUFA arm should be interpreted as EPA/DHA enrichment
277 within a MUFA-rich dietary context rather than as the effect of fish oil alone. This formulation
278 is not expected to compromise ω 3 bioavailability and may improve dietary stability and
279 comparability among groups. The relative advantage of EVOO over refined MUFA suggests
280 that food matrix components can amplify benefits beyond oleate content per se. Two
281 considerations temper interpretation. First, FJC identifies ongoing degeneration but does not
282 specify death pathways; pairing FJC with neuronal markers (e.g., NeuN) and
283 apoptosis/oxidative readouts would refine attribution. Second, the scopolamine window is short
284 and high-amplitude; extending dietary exposure, lengthening the post-challenge interval, and
285 increasing group size would improve sensitivity to resolve differences between MUFA sources
286 and to determine whether SFA-associated vulnerability persists or escalates.²⁶ Even with these
287 boundaries, the convergence of body-weight patterns and FJC burden supports the conclusion
288 that dietary fat quality and matrix shape systemic status and buffer acute neurodegeneration,
289 with EVOO showing the most favourable profile and ω 3-LCPUFA a close second.





290

291 **Figure 2. Fluoro-Jade C identifies scopolamine-evoked neurodegeneration with diet-dependent modulation in**
 292 **the dentate gyrus. (A) Representative FJC/DAPI micrographs (arrows highlight FJC-positive degenerating profiles)**
 293 **and (B) quantification across SD, SD-SCO, HFD-MUFA (EVOO), HFD-rMUFA (ROO), HFD-SFA (RPO), and HFD-**
 294 **ω 3-LCPUFA. Scopolamine increased FJC-positive signal relative to SD, whereas ω 3-LCPUFA and EVOO showed**
 295 **the lowest values among HFDs, with SFA tending higher; exact *p*-values for significant contrasts are reported on the**
 296 **plot. Quantification was performed blinded on anatomically matched dentate-gyrus ROIs (three sections per mouse; *n***
 297 **= 3–4 mice per group) under identical acquisition settings. Y-axis: FJC-positive area (%).**

298 3.2. Microglial activation and inflammatory effectors are dampened by HFDs but show 299 limited separation across lipid classes under scopolamine stress

300 In the dentate gyrus, scopolamine elicited the expected inflammatory surge, with higher
 301 densities of Iba-1+, TNF- α + and COX-2+ profiles in SD-SCO versus SD, consistent with a rapid
 302 shift toward a reactive microglial milieu under acute cholinergic stress (**Figure 3**, representative
 303 TNF- α and COX-2 micrographs in **Supplementary Material-Figures S2–S3**). Across all
 304 HFDs, this increase was significantly blunted relative to SD-SCO, bringing all three markers
 305 closer to SD values; however, pairwise contrasts among HFDs were not significant (one-way



ANOVA/Tukey), indicating that in this short, high-amplitude window a dominant high-fat exposure effects overrides finer distinctions attributable to fatty acid class. At the marker level, Iba-1 reductions indicate fewer microglia in an activated state; although Iba-1 is not state-exclusive, it remains a widely used readout of microglial presence/reactivity in brain tissue.²⁷ Lower TNF- α aligns with curtailed cytokine signalling that perturbs synaptic function and plasticity during neuroinflammation, offering a parsimonious explanation for the attenuated effector milieu in HFD groups.²⁸ The decline in COX-2 is compatible with damping of the eicosanoid/oxidative arm of the response in hippocampus, where COX-2 activity influences neuronal excitability and network dynamics.²⁹ The concordant directionality across these independent readouts argues for a coordinated dampening rather than assay-specific variance or thresholding artefacts and is supported by identical acquisition settings and blinded quantification in matched hippocampal sections. Mechanistically, the absence of separation among HFD classes under acute scopolamine likely reflects compression of between-group variance by a brief, high-amplitude insult, together with the inherently coarse granularity of density-based IHC markers for detecting second-order lipid-class effects. Extending the dietary exposure and the post-challenge interval, and increasing group size, particularly for histological endpoints, are recommended to resolve subtler differences between MUFA sources and to determine whether SFA-associated vulnerability persists or escalates in longer windows of observation.

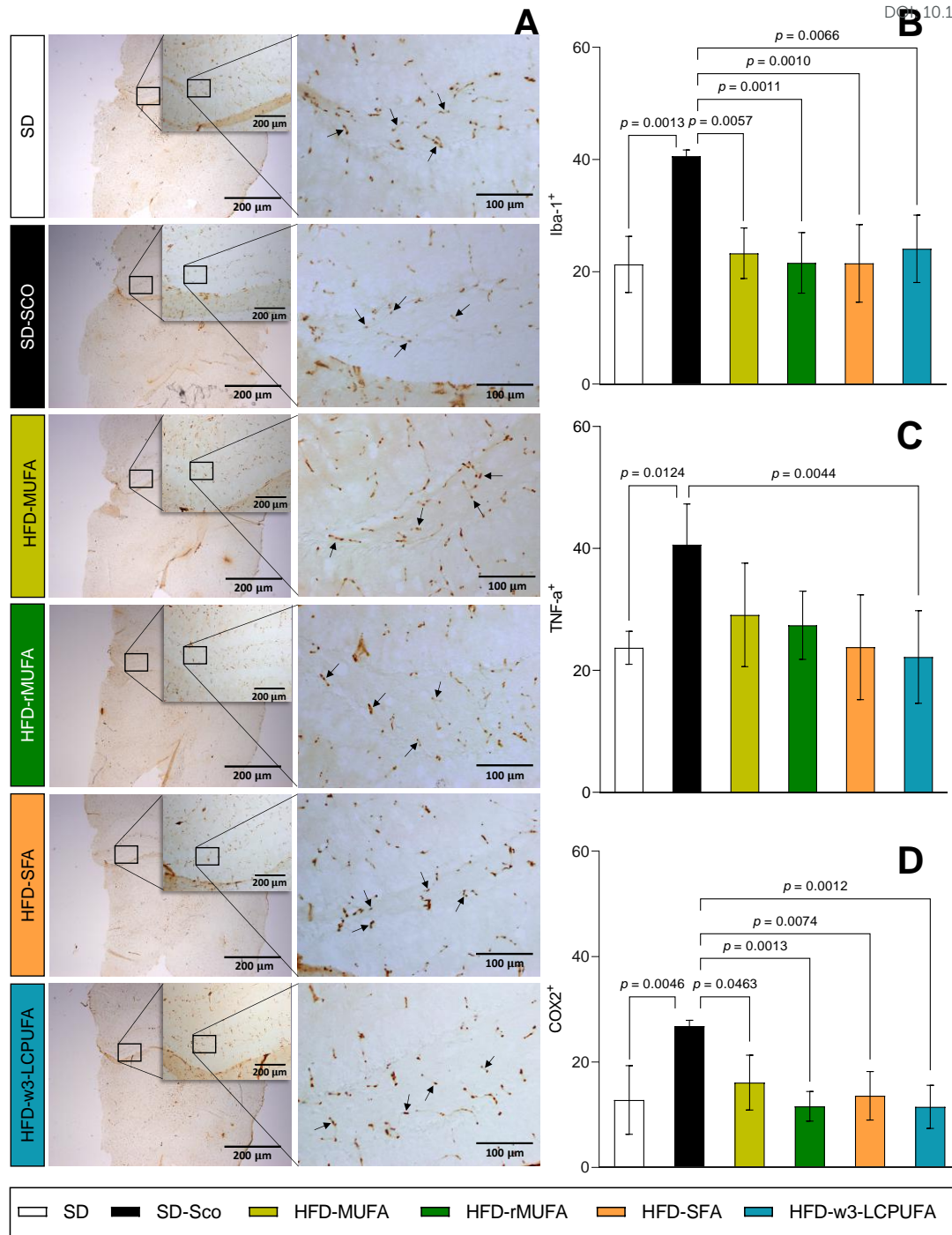
Although pairwise contrasts among HFDs did not reach significance, the bar patterns consistently suggest ω 3-LCPUFA at or near the lowest inflammatory values, with EVOO frequently trending below ROO and SFA. Two features likely obscured class effects. First, acute scopolamine delivers a steep, rapidly resolving neuroimmune pulse that can compress variance and floor between-diet differences once any HFD is present.²⁶ Second, density-based IHC metrics (Iba-1/COX-2/TNF- α), while appropriate for detecting large state shifts, are intrinsically less sensitive than morphology-aware descriptors (e.g., process complexity, convex hull, nearest-neighbour spacing) for capturing lipid-class influences.³⁰ This reading is congruent with our astroglial IF, where GFAP intensity and shape descriptors show clearer gradient (ω 3-LCPUFA > EVOO-MUFA \approx rMUFA > SFA), implying that astrocytes are earlier or more sensitive integrators of dietary lipid cues, whereas microglia display a shared buffering under the present acute paradigm. Mechanistically, several non-exclusive routes could account for the HFD-wide attenuation. Systemically, high-fat feeding remodels endocrine and adipokine profiles and stress physiology, potentially resetting brain immune set-points before the cholinergic challenge.³¹ At the cellular level, even short exposures can recompense membrane lipids and raft architecture, adjusting receptor thresholds and signalling gain; such rapid remodelling would favour a class-agnostic reduction when the insult is brief.³² In parallel, gut–



342 brain communication, including microbial metabolites and vagal inputs, may converge on
343 hippocampal microglia to limit peak responses.³³ While our design does not disentangle these
344 pathways, the internal consistency across markers supports a shared upstream influence during
345 the scopolamine window. Importantly, the docking layer provides target-level plausibility for
346 quality-dependent effects that may require longer exposure or progressive pathology to become
347 histologically apparent: EPA/DHA showed the most favourable engagement at COX-2 and
348 BACE1, and long-chain fatty acids occupied the AChE peripheral site and a TREM2 lipid/apoE-
349 responsive interface, outlining biochemical routes by which ω 3-rich or EVOO-based diets could
350 differentially modulate eicosanoid, amyloidogenic, cholinergic and microglial-sensing axes
351 even if such separations do not yet reach significance among HFDs in this acute model.
352 Together, these considerations support a two-tier interpretation: a broad, short-term buffering of
353 scopolamine-induced microglial activation common to all HFDs that collapses between-diet
354 differences in Iba-1/COX-2/TNF- α densities; and diet-quality-sensitive modulation that
355 emerges more clearly in astrocyte metrics and is foreshadowed by *in silico* target engagement.
356 To increase microglial resolution, future studies should increase histological sample sizes,
357 extend the dietary intervention and post-challenge windows, incorporate morphology- and
358 spatially aware microglial analytics, and pair histology with hippocampal lipid-mediator
359 profiling (COX-2-linked prostanoids and specialised pro-resolving mediators) to test whether
360 the predicted docking hierarchy is mirrored by shifts in eicosanoid networks.

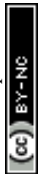
View Article Online
DOI: 10.1039/D6FO00279J





361

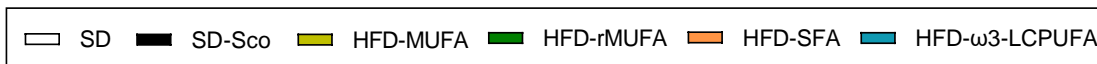
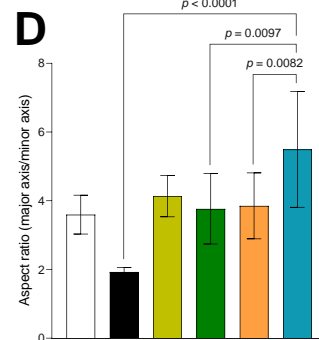
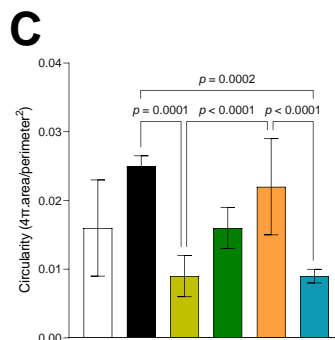
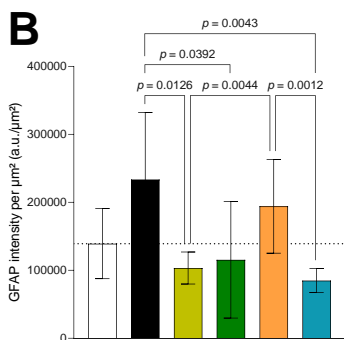
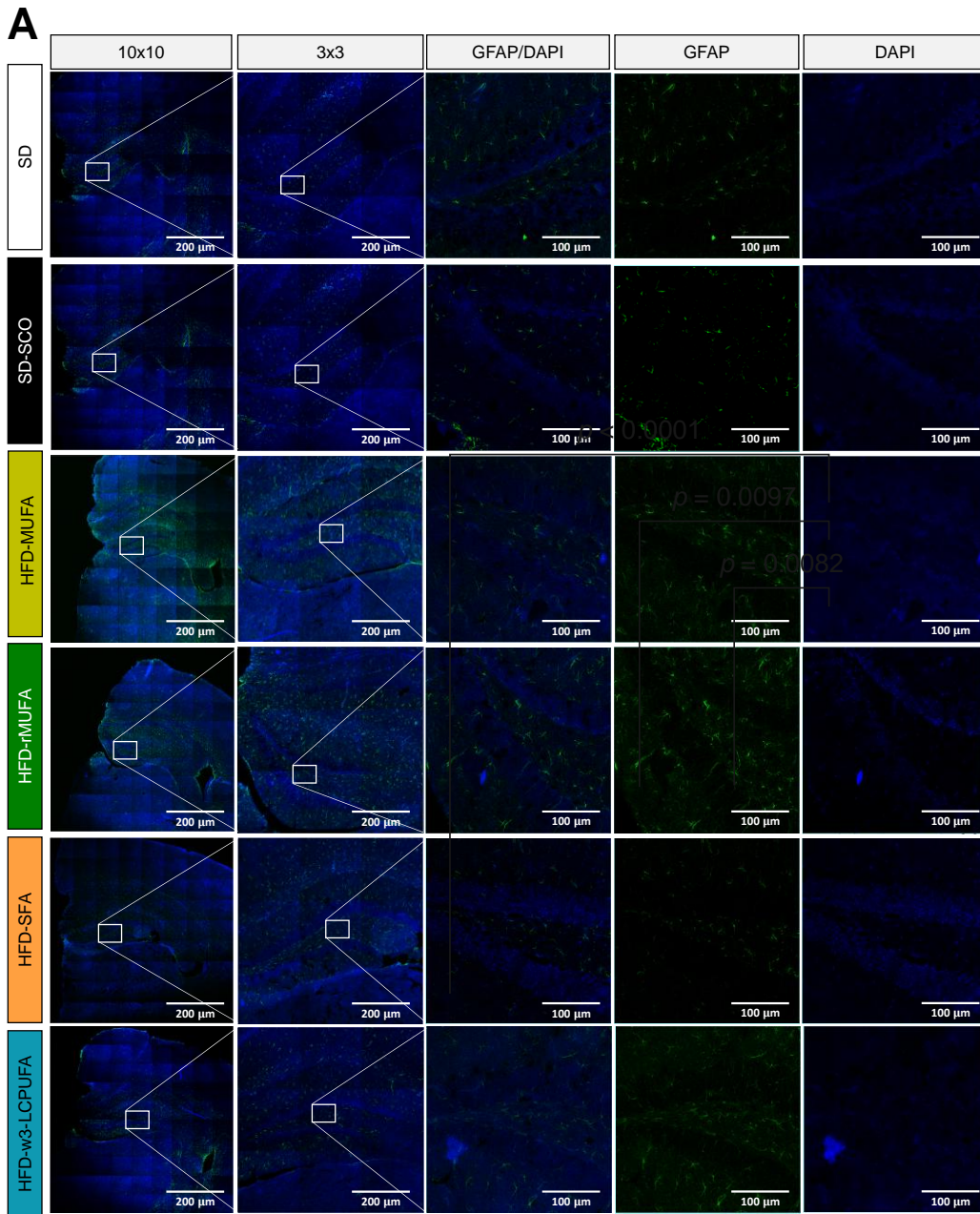
362 **Figure 3. High-fat diets attenuate scopolamine-evoked microglial and inflammatory markers in the dentate**
 363 **gyrus. (A)** Representative IHC micrographs (left; low-magnification overview with inset; right: high-magnification
 364 ROI) and quantification for **(B)** Iba-1, **(C)** TNF- α , and **(D)** COX-2 across SD, SD-SCO, HFD-MUFA (EVOO), HFD-
 365 rMUFA (ROO), HFD-SFA (RPO), and HFD- ω 3-LCPUFA. Arrows indicate representative Iba-1-positive profiles
 366 within the dentate gyrus (brown DAB signal). Quantification was performed blinded on anatomically matched
 367 dentate gyrus sections (three sections per mouse). Data are mean \pm SD; one-way ANOVA with Tukey's post hoc test.
 368 Exact *p*-values for significant contrasts are reported on the plots. Scale bars: 200 μ m (overview), 100 μ m (insets).



369 3.3. Astrocyte reactivity tracks dietary fat quality and aligns with omega-3 enrichment and 370 EVOO matrix effects

371 IF for GFAP in the dentate gyrus revealed a clear, diet-dependent modulation of astrocyte
372 reactivity under scopolamine (**Figure 4**). Relative to SD, SD-Sco showed higher GFAP intensity
373 and a shift toward a hypertrophic morphology, greater circularity and lower aspect ratio,
374 consistent with swollen, less-ramified astrocytes. All HFDs reduced this response to some
375 extent, but the magnitude followed a consistent hierarchy. HFD- ω 3-LCPUFA displayed the
376 lowest GFAP signal among HFDs ($p = 0.0043$ vs HFD-SFA) and the most favourable
377 morphology (reduced circularity, $p < 0.0001$; increased aspect ratio, $p = 0.0082$; both vs HFD-
378 SFA), with HFD-MUFA (EVOO) as close second. HFD-rMUFA occupied an intermediate
379 position, whereas HFD-SFA showed the smallest improvement and frequently remained closest
380 to SD-Sco. Taken together, the gradient ω 3-LCPUFA > EVOO > rMUFA > SFA across three
381 orthogonal GFAP metrics (integrated intensity per area, circularity, and aspect ratio) supports
382 the view that fat quality, and, specifically, omega-3 enrichment and the EVOO matrix,
383 meaningfully modulates astrocyte state during an acute cholinergic challenge. Several non-
384 exclusive factors could account for this pattern. First, lipid class-dependent membrane
385 remodelling may influence astrocytic calcium dynamics,³⁴ gap-junction coupling,³⁵ and
386 susceptibility to oxidative stress;³⁶ with long-chain ω 3 chains favouring a more compliant
387 bilayer than SFA-rich profiles. Second, bioactive phenolics present in EVOO but largely absent
388 from refined oils can provide additional antioxidant and anti-inflammatory buffering, either
389 directly within astrocytes or indirectly via the perivascular niche, facilitating restoration of a
390 more ramified/physiologic morphology.³⁷ Third, diet-driven systemic cues (energy balance,
391 adipokines, stress hormones) plausibly shift astroglial set-points and thereby alter the magnitude
392 of the acute response to scopolamine.²⁵ Methodologically, the convergence of intensity and
393 morphology metrics, together with uniform acquisition parameters and blinded quantification on
394 matched sections, argues against threshold artefacts and supports a genuine biological
395 separation among diets. The present readouts capture structural reactivity (GFAP load and shape
396 descriptors) rather than pathway specificity; pairing morphology with indices of astrocytic
397 metabolism (e.g., glutamate transporters, antioxidative enzymes) or live-cell indicators of
398 calcium dynamics would refine mechanistic inference. In addition, the observation window is
399 short; extending dietary exposure and the post-challenge interval would help to test the
400 durability of the EVOO advantage over refined MUFA, and to determine whether ω 3-LCPUFA
401 and EVOO exert additive or mechanistically distinct modes of astroglial control. Even within
402 these bounds, Figure 4 demonstrates that dietary fat quality and matrix strongly condition
403 astrocyte responses to cholinergic stress, with ω 3-LCPUFA showing the most favourable profile
404 and EVOO a close second, whereas SFA confers the least protection.





407 **Figure 4. Astrocyte reactivity is diet-dependent under scopolamine.** (A) Representative confocal images of the
 408 dentate gyrus (columns: 10×10 overview, 3×3 zoom, GFAP/DAPI merge, GFAP channel, DAPI channel) and (B)
 409 quantification of GFAP intensity per μm^2 (a.u./ μm^2), (C) circularity ($4\pi \cdot \text{area}/\text{perimeter}^2$), and (D) aspect ratio (major
 410 axis/minor axis) across SD, SD-Sco, HFD-MUFA (EVOO), HFD-rMUFA (ROO), HFD-SFA (RPO), and HFD- ω 3-
 411 LCPUFA. Scopolamine increased GFAP intensity and drove hypertrophic, less-elongated astrocytes (higher
 412 circularity, lower aspect ratio) relative to SD. All HFDs mitigated this response, with ω 3-LCPUFA showing the
 413 lowest GFAP signal and most favourable morphology, followed by EVOO, then rMUFA, and SFA. Exact *p*-values for
 414 significant contrasts are shown on the plots. Imaging was performed under identical acquisition settings;
 415 quantification was blinded on anatomically matched sections (three sections per mouse). Scale bars: 200 μm
 416 (overview), 100 μm (zoom and single-channel panels).

417 3.4. Molecular docking suggests a biochemical rationale for PUFA superiority and EVOO 418 advantages

419 The docking dataset outlines a coherent target-level framework that mirrors the *in vivo*
 420 hierarchy, DHA/EPA > oleic \geq palmitic, and offers mechanistic nuances for why ω 3-LCPUFA
 421 feeding and, secondarily, olive oil matrices confer advantages. Across AChE, TREM2, BACE-1,
 422 and COX-2, DHA and EPA yielded the most favourable predicted binding free energies (Table
 423 1), while oleic acid occupied functionally relevant surfaces with intermediate scores and
 424 palmitic acid generally trailed, consisted with a more limited interaction repertoire dominated
 425 by apolar fit. For AChE, which governs synaptic acetylcholine tone in the scopolamine
 426 paradigm,³⁸ DHA ($-7.4 \text{ kcal mol}^{-1}$) and EPA ($-7.6 \text{ kcal mol}^{-1}$) outperformed oleic (-5.9 kcal
 427 mol^{-1}) and palmitic ($-6.5 \text{ kcal mol}^{-1}$). Poses clustered in the peripheral anionic site (PAS) rather
 428 than establishing a credible catalytic geometry at the Ser203-His447-Glu334 triad; all ligands
 429 engaged canonical PAS residues (e.g., Tyr72, Trp86, Tyr124, Trp286, Phe295, Tyr337, Phe338),
 430 whereas only the SFAs/MUFAs occasionally approached the triad without forming catalytically
 431 competent contacts (Figure 5).³⁹ This PAS-biased pattern suggests non-catalytic modulation, a
 432 plausible route to mitigate scopolamine-evoked dysfunction, rather than classical active site
 433 inhibition, thus providing a mechanistic bridge to the cholinergic layer of our *in vivo* readouts.

434 **Table 1.** Predicted binding free energies (ΔG , kcal mol^{-1}) for dietary fatty acids docked to AChE, TREM2, BACE1,
 435 and COX-2. Values correspond to the best-scoring pose per complex; more negative indicates stronger predicted
 436 binding.

Target	Ligand			
	Palmitic acid (C16:0)	Oleic acid (C18:1 ω 9)	EPA (C20:5 ω 3)	DHA (C22:6 ω 3)
AChE	-6.5	-5.9	-7.6	-7.4
TREM2	-7.7	-7.7	-8.0	-7.4
BACE1	-6.8	-6.9	-8.4	-8.5
COX-2	-8.3	-9.2	-9.8	-10.5

437 Abbreviations: AChE, acetylcholinesterase; BACE1, β -site APP cleaving enzyme 1; COX-2, cyclooxygenase-2;
 438 TREM2, triggering receptor expressed on myeloid cells 2; EPA, eicosapentaenoic acid; DHA, docosahexaenoic acid.



439 For TREM2, all fatty acids localized to the apoE-interacting surface of the ectodomain, a lipid
440 sensing patch implicated in agonist responses;²¹ EPA ($-8.0 \text{ kcal mol}^{-1}$) scored highest, with oleic
441 and palmitic ($-7.7 \text{ kcal mol}^{-1}$), and DHA ($-7.4 \text{ kcal mol}^{-1}$) close behind (**Figure 6**). Although
442 top-ranked poses did not form a specific salt bridge to Arg47, their consistent occupancy of this
443 agonist-responsive interface is compatible with allosteric stabilization of microglial TREM2
444 signalling. This aligns with the broadly reduced microglial markers observed across HFDs and
445 suggests that quality-dependent differences may require longer exposure or disease-progressive
446 models to surface histologically. For BACE1, the aspartyl protease that initiates the
447 amyloidogenic pathway by cleaving APP at the β -site, ultimately leading to the formation of
448 amyloid- β peptides,⁴⁰ EPA ($-8.4 \text{ kcal mol}^{-1}$) and DHA ($-8.5 \text{ kcal mol}^{-1}$) again surpassed oleic
449 ($-6.9 \text{ kcal mol}^{-1}$) and palmitic ($-6.8 \text{ kcal mol}^{-1}$) (**Figure 7**). Poses occupied the catalytic cleft but
450 primarily made van der Waals contacts with the Asp32-Asp228 dyad, while establishing
451 interactions with lining residues (e.g., Thr72 hydrogen bonds; Phe108 π -alkyl/aromatic
452 contacts).⁴¹ This is compatible with substrate-gating or micro-allosteric effects rather than tight
453 competitive inhibition, consistent with a scenario in which ω 3-LCPUFA-rich environments
454 subtly influence APP processing in concert with membrane remodelling. Finally, COX-2
455 displayed the strongest absolute scores, led by DHA ($-10.5 \text{ kcal mol}^{-1}$) and EPA ($-9.8 \text{ kcal mol}^{-1}$);
456 notably oleic ($-9.2 \text{ kcal mol}^{-1}$) also docked favourably relative to palmitic ($-8.3 \text{ kcal mol}^{-1}$)
457 within arachidonate-binding channel (**Figure 8**). Ligands engaged a network of hydrophobic
458 and aromatic contacts (including Trp387, among others)⁴² and carboxylate-compatible
459 interactions near the channel entrance. The rank order across with the notion that highly
460 unsaturated chains exploit the elongated channel more efficiently, offering a target-level
461 rationale for eicosanoid/resolution pathway modulation under ω 3-LCPUFA feeding.⁴³
462 Collectively, this composition, binding, and function chain strengthens the translational
463 rationale for prioritizing ω 3-LCPUFA and high-quality olive oils as dietary strategies to
464 modulate neuroinflammatory and amyloid-relevant axis *in vivo*, while underscoring the need for
465 biophysical and biochemical validation in membrane-mimetic systems to refine these
466 interaction maps.

467

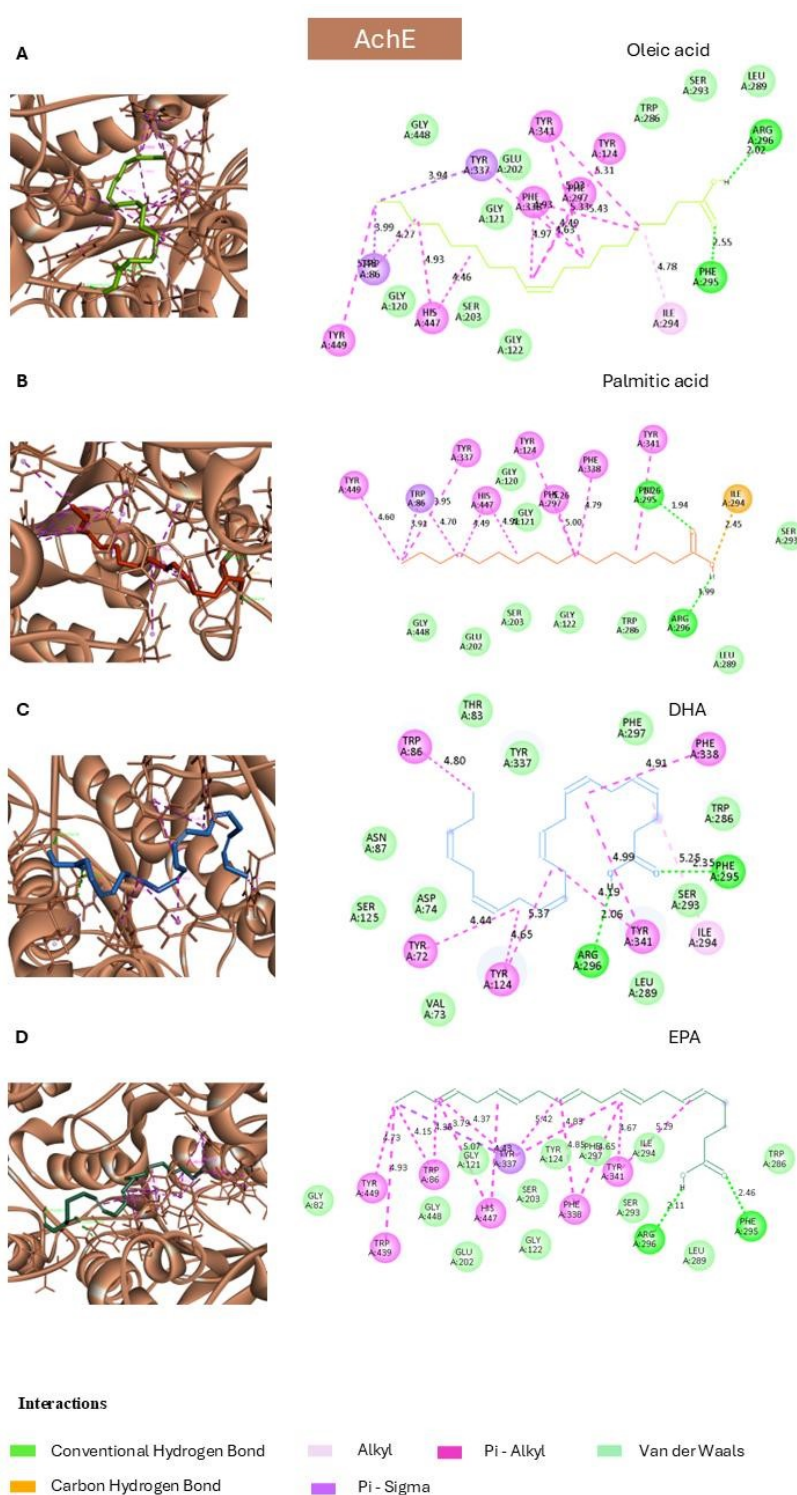
468

469

470

471

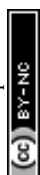


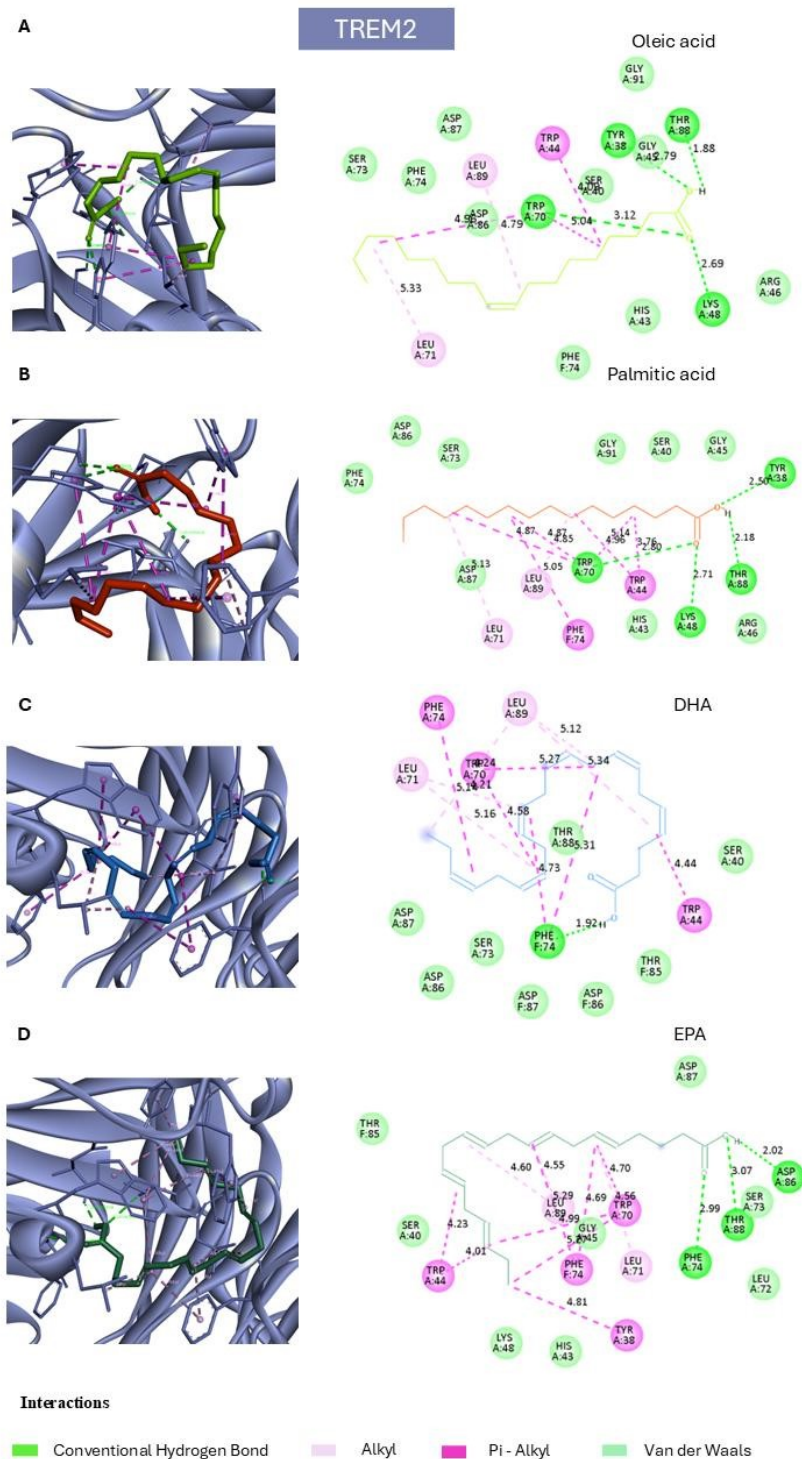


View Article Online
DOI: 10.1039/D6FO00279J

472

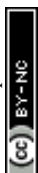
473 **Figure 5. Binding poses and interaction fingerprints of dietary fatty acids in the acetylcholinesterase (AChE;**
 474 **PDB 5DTI) active-site gorge.** Left panels: best-scoring docked poses within the AChE binding gorge. Right panels:
 475 corresponding 2D interaction diagrams (hydrogen bonds, π /alkyl contacts, van der Waals) generated in BIOVIA
 476 Discovery Studio Visualizer. (A) Oleic acid–AChE; (B) Palmitic acid–AChE; (C) DHA–AChE; (D) EPA–AChE.
 477 Poses predominantly occupy the peripheral anionic site (PAS) region, with occasional proximity to the catalytic triad
 478 (Ser203–His447–Glu334), consistent with PAS-biased engagement rather than direct catalytic geometry. All images
 479 were produced using identical visualization settings.

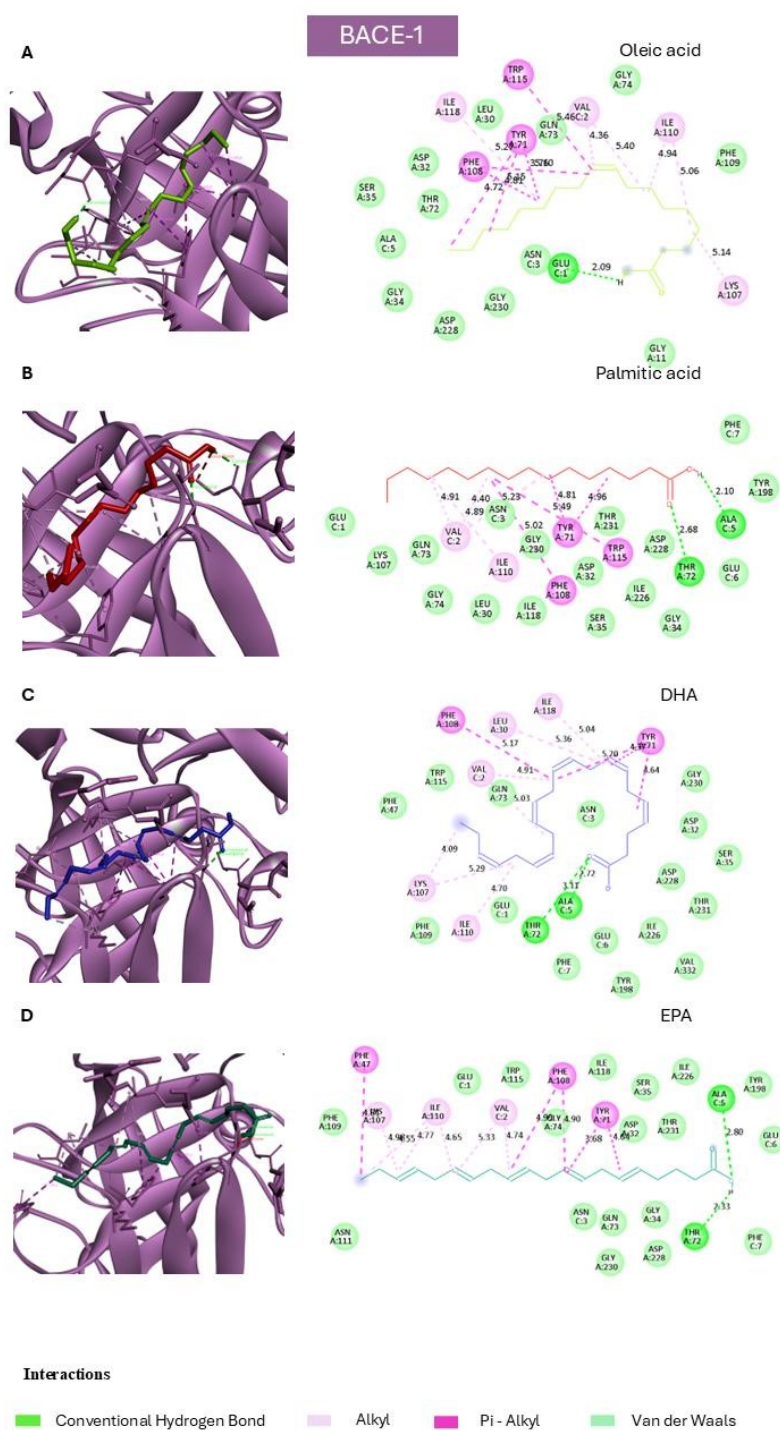




480

481 **Figure 6. Binding poses and interaction fingerprints of dietary fatty acids at the TREM2 (PDB 5UD7)**
 482 **ectodomain surface.** Left panels: best-scoring docked poses on the apoE-interacting, agonist-responsive interface of
 483 TREM2. Right panels: corresponding 2D interaction diagrams (hydrogen bonds, π /alkyl and alkyl contacts, van der
 484 Waals) generated in BIOVIA Discovery Studio Visualizer. (A) Oleic acid–TREM2; (B) Palmitic acid–TREM2; (C)
 485 DHA–TREM2; (D) EPA–TREM2. Top-ranked poses consistently occupy the lipid/apoE-responsive surface; specific
 486 Arg47 salt bridges were not observed in the best poses, but engagement of the same functional patch supports a
 487 putative allosteric stabilization of TREM2 signalling. All renderings used identical visualization parameters.



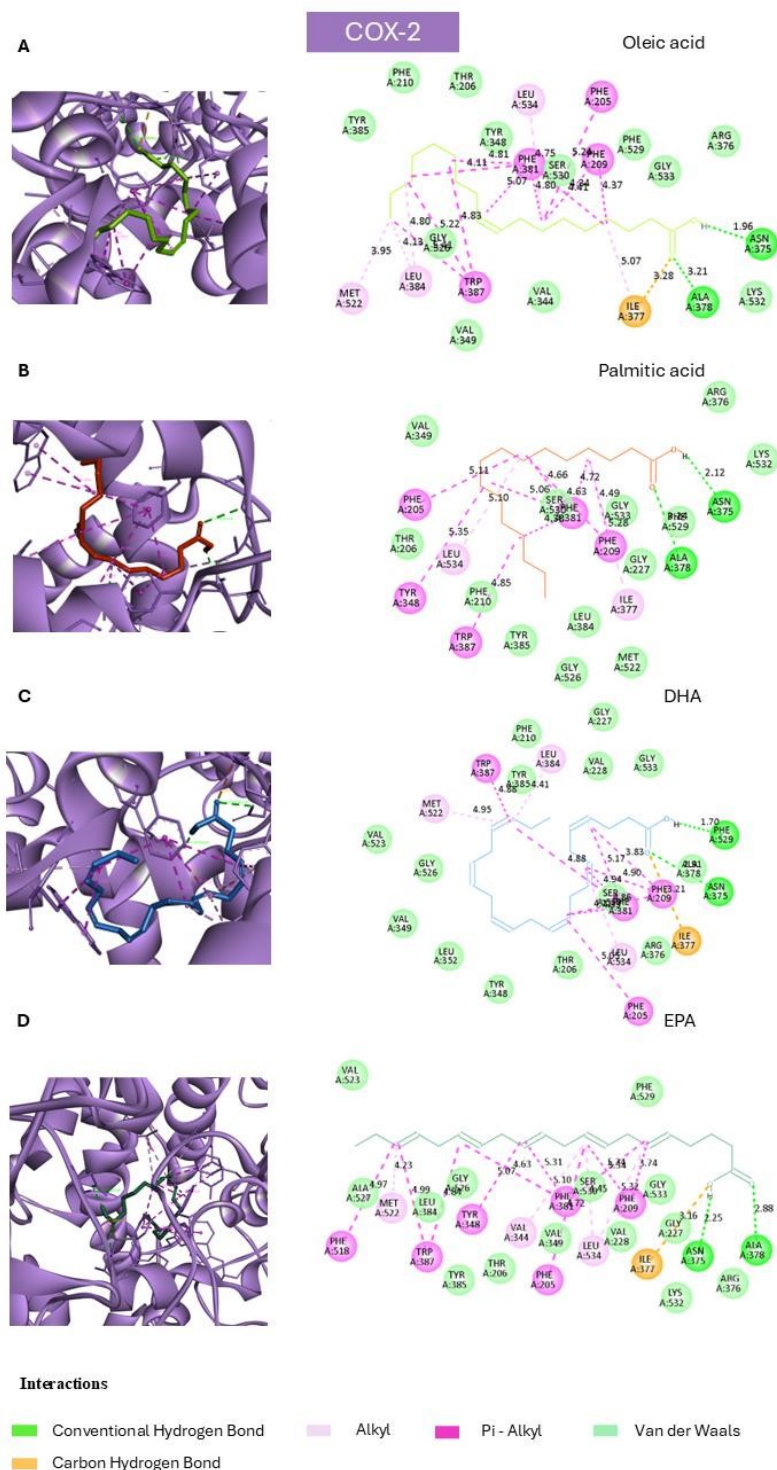


View Article Online
DOI: 10.1039/D6FO00279J

488

489 **Figure 7 Binding poses and interaction fingerprints of dietary fatty acids in the β -secretase 1 (BACE1; PDB**
 490 **1FKN) catalytic cleft.** Left panels: best-scoring docked poses within the active site of BACE1. Right panels:
 491 corresponding 2D interaction diagrams (hydrogen bonds, π /alkyl and alkyl contacts, van der Waals) generated in
 492 BIOVIA Discovery Studio Visualizer. (A) Oleic acid–BACE1; (B) Palmitic acid–BACE1; (C) DHA–BACE1; (D)
 493 EPA–BACE1. Poses occupy the catalytic cleft with predominant contacts to lining residues (e.g., Thr72, Phe108) and
 494 mainly van der Waals proximity to the Asp32–Asp228 catalytic dyad, consistent with substrate-gating/micro-
 495 allosteric engagement rather than tight competitive inhibition. All renderings used identical visualization parameters.





496

497 **Figure 8. Binding poses and interaction fingerprints of dietary fatty acids in the cyclooxygenase-2 (COX-2;**
 498 **PDB 1DDX) arachidonic-acid channel.** Left panels: best-scoring docked poses within the arachidonate-binding
 499 channel of COX-2. Right panels: corresponding 2D interaction diagrams (hydrogen bonds, π /alkyl and alkyl contacts,
 500 van der Waals) generated in BIOVIA Discovery Studio Visualizer. (A) Oleic acid–COX-2; (B) Palmitic acid–COX-2;
 501 (C) DHA–COX-2; (D) EPA–COX-2. Poses occupy the elongated hydrophobic channel with engagement of lining
 502 residues consistent with arachidonate accommodation, in line with a non-covalent, channel-filling binding mode. All
 503 renderings used identical visualization parameters.



504 4. CONCLUSIONS

505 Dietary fat quality, beyond total fat, emerged as a key determinant of brain immune tone in a
506 scopolamine-induced, Alzheimer's-like context. ω 3-LCPUFA feeding consistently dampened
507 astroglial reactivity and restored a more physiological, ramified morphology, while EVOO-
508 MUFA conferred advantages over refined MUFA, consistent with matrix/phenolic co-factors.
509 By contrast, microglial markers (Iba-1, TNF- α , COX-2) were broadly attenuated across HFDs,
510 suggesting a dominant effect of lipid availability on acute neuroinflammatory set-points in this
511 short, high-amplitude window. Complementary structure-based docking offered a mechanistic
512 scaffold: EPA/DHA showed the strongest predicted engagement at COX-2 and BACE1,
513 whereas MUFA/SFA populated functionally relevant regions on AChE (PAS) and TREM2
514 (apoE-responsive surface), outlining plausible eicosanoid, amyloid, cholinergic and microglial-
515 sensing axes by which diet can shape neuroimmune signalling. Together, these lines of evidence
516 support a composition, binding, and function framework in which PUFA-rich and EVOO-based
517 diets buffer neuroinflammation pertinent to AD. This work has boundaries, notably an acute
518 cholinergic paradigm, rigid-receptor docking without explicit membranes, and limited readouts
519 of neuronal integrity, but the internal directionality is coherent and actionable. We propose
520 targeted lipidomics and eicosanoid/pro-resolving mediator profiling to test whether COX-2-
521 linked networks mirror the predicted hierarchy; TREM2 signalling assays and BACE1
522 enzymology in progressive amyloid/tau models to examine causality; and factorial designs
523 separating fatty-acid class from EVOO phenolics to quantify matrix co-drivers. A limitation is
524 that EPA/DHA were administered in combination with a MUFA-rich oil (ROO), which
525 increases nutritional realism but does not allow us to isolate the effect of fish oil as the sole fat
526 source. Overall, the findings strengthen the translational rationale for precision nutrition
527 strategies prioritising ω 3-LCPUFA and high-quality olive oils to modulate neuroinflammation
528 and potentially slow trajectories relevant to AD.

529

530 Author Contributions

531 Conceptualization, C.M.C.-C., S.M.-d.l.P.; methodology, L.B.-C, M.A., T.G.-d.l.R, M.D.N-H;
532 formal analysis, T.G.-d.l.R., E.M.-P., M.T.-L.; investigation, J.L.d.l.R.-V, T.G.-d.l.R., S.M.-d.l.P.;
533 resources, S.M.-d.l.P.; writing—original draft preparation, M.A.; writing— review and editing,
534 S.M.-d.l.P; supervision, S.M.-d.l.P.; funding acquisition, S.M.-d.l.P.. All authors have read and
535 agreed to the published version of the manuscript. All authors have read and agreed to the
536 published version of the manuscript.

537



538

539 Acknowledgements

540 Luna Barrera-Chamorro has the benefit of doctoral fellowship supported by the VII Program of
541 Inner Initiative for Research and Transfer of University of Seville (VII-PPIT-US). Teresa
542 Gonzalez-de la Rosa, Maria Torrecillas-Lopez, and Elvira Marquez-Paradas has the benefit of a
543 doctoral fellowship from the Spanish Ministry of Science, Innovation, and Universities
544 (FPU23/02652, PREP2022–000408, FPU22/01097, respectively). Jose L. del-Rio-Vazquez is
545 supported by a research contract funded by the project PID2022-138650OA-I00, granted by
546 MCIN/AEI/10.13039/501100011033. Maria D. Navarro-Hortal is supported by a Juan de la
547 Cierva Grant with reference number JDC2023-050414-I, funded by
548 AEI/10.13039/501100011033 and the FSE+.

549 Funding

550 This publication is part of the project PID2022-138650OAI00, funded by
551 MICIU/AEI/10.13039/501100011033 and by ERDF/EU.

552 Declaration of competing interest

553 The authors declare that they have no known competing financial interests or personal
554 relationships that could have appeared to influence the work reported in this paper.

555

556

557

558

559

560

561

562

563

564

565

566



567

View Article Online
DOI: 10.1039/D6FO00279J

568 REFERENCES

- 569 1. J. P. Ferrari-Souza, G. Povala, N. Rahmouni, B. Bellaver, P. C. L. Ferreira, M. A. De Bastiani,
570 et al., Microglia modulate A β -dependent astrocyte reactivity in Alzheimer's disease, *Nat.*
571 *Neurosci.*, **2026**, 29, 81-87, DOI: 10.1038/s41593-025-02103-0.
- 572 2. F. Yin, Lipid metabolism and Alzheimer's disease: clinical evidence, mechanistic link and
573 therapeutic promise, *FEBS J.*, **2023**, 290, 1420–1453, DOI: 10.1111/febs.16344.
- 574 3. E. Grao-Cruces, C. M. Claro-Cala, S. Montserrat-de la Paz, C. Nóbrega, Lipoprotein
575 metabolism, protein aggregation, and Alzheimer's disease: a literature review, *Int. J. Mol. Sci.*,
576 **2023**, 24, 2944, DOI: 10.3390/ijms24032944.
- 577 4. F. Rivero-Pino, E. Grao-Cruces, S. Lopez-Enriquez, G. Alba, E. Marquez-Paradas, C. M.
578 Claro-Cala, C. Santa-Maria, S. Montserrat-de la Paz, Modulation of beta-amyloid-activated
579 primary human neutrophils by dietary phenols from virgin olive oil, *Nutrients*, **2023**, 15, 941,
580 DOI: 10.3390/nu15040941.
- 581 5. R. Toscano, M. C. Millan-Linares, A. Lemus-Conejo, C. Claro, V. Sanchez-Margalet, S.
582 Montserrat-de la Paz, Postprandial triglyceride-rich lipoproteins promote M1/M2 microglia
583 polarization in a fatty-acid-dependent manner, *J. Nutr. Biochem.*, **2020**, 75, 108248, DOI:
584 10.1016/j.jnutbio.2019.108248.
- 585 6. A.-J. Tessier, M. Cortese, C. Yuan, K. Bjornevik, A. Ascherio, D. D. Wang, J. E. Chavarro, M.
586 J. Stampfer, F. B. Hu, W. C. Willett, M. Guasch-Ferré, Consumption of olive oil and diet quality
587 and risk of dementia-related death, *JAMA Netw. Open*, **2024**, 7, e2410021, DOI:
588 10.1001/jamanetworkopen.2024.10021.
- 589 7. M. Poxleitner, S. H. L. Hoffmann, G. Berezhnoy, T. M. Ionescu, I. Gonzalez-Menendez, F. C.
590 Maier, et al., Western diet increases brain metabolism and adaptive immune responses in a
591 mouse model of amyloidosis, *J. Neuroinflammation*, **2024**, 21, 129, DOI: 10.1186/s12974-024-
592 03080-0.
- 593 8. L. Barrera-Chamorro, A. Fernandez-Prior, C. M. Claro-Cala, J. L. del Rio-Vazquez, F.
594 Rivero-Pino, S. Montserrat-de la Paz, Unveiling the neuroprotective impact of virgin olive oil
595 ingestion via the microbiota–gut–brain axis, *Food Funct.*, **2025**, 16, 24–39, DOI:
596 10.1039/D4FO04560B.
- 597 9. M. E. Traetta, H. A. Vecchiarelli, M.-È. Tremblay, Fundamental neurochemistry review:
598 lipids across microglial states, *J. Neurochem.*, **2025**, 169, e16259, DOI: 10.1111/jnc.16259.



- 599 **10.** M. Slayo, C. Rummel, P. H. Singhaarachchi, M. Feldotto, S. J. Spencer, The role of n-3
600 derived specialised pro-resolving mediators (SPMs) in microglial mitochondrial respiration and
601 inflammation resolution in Alzheimer's disease, *Mol. Neurodegener.*, **2025**, *20*, 35, DOI:
602 10.1186/s13024-025-00824-1.
- 603 **11.** Y. Chen, R. Touboul, Y. Chen, C. L. Chang, Strategic delivery of omega-3 fatty acids for
604 modulating inflammatory neurodegenerative diseases, *Front. Aging Neurosci.*, **2025**, *17*,
605 1535094, DOI: 10.3389/fnagi.2025.1535094.
- 606 **12.** A. Cañuelo, Olive polyphenols as modulators of amyloid aggregation: mechanisms and
607 implications for neurodegenerative diseases, *Food Funct.*, **2025**, *16*, 8658–8679, DOI:
608 10.1039/D5FO03331D.
- 609 **13.** F. Rivero-Pino, Oleocanthal – characterization, production, safety, functionality and in vivo
610 evidences, *Food Chem.*, **2023**, *425*, 136504, DOI: 10.1016/j.foodchem.2023.136504.
- 611 **14.** R. Zupo, F. Castellana, F. Panza, V. Solfrizzi, M. Lozupone, R. Tardugno, et al., Alzheimer's
612 disease may benefit from olive oil polyphenols: a systematic review on preclinical evidence
613 supporting the effect of oleocanthal on amyloid- β load, *Curr. Neuropharmacol.*, **2025**, *23*,
614 1249–1259, DOI: 10.2174/011570159X327650241021115228.
- 615 **15.** G. C. De Paula, B. I. Aldana, R. Battistella, R. Fernández-Calle, A. Bjure, I. Lundgaard, T.
616 Deierborg, J. M. N. Duarte, Extracellular vesicles released from microglia after palmitate
617 exposure impact brain function, *J. Neuroinflammation*, **2024**, *21*, 173, DOI: 10.1186/s12974-
618 024-03168-7.
- 619 **16.** P. Prakash, C. E. Randolph, K. A. Walker, G. Chopra, Lipids: emerging players of microglial
620 biology, *Glia*, **2025**, *73*, 657–677, DOI: 10.1002/glia.24654.
- 621 **17.** S. De Chiara, L. De Simone Carone, R. Cirella, E. Andretta, A. Silipo, A. Molinaro, M.
622 Mercogliano, F. Di Lorenzo, Beyond the Toll-like receptor 4: structure-dependent
623 lipopolysaccharide recognition systems—how far are we?, *ChemMedChem*, **2025**, *20*,
624 e202400780, DOI: 10.1002/cmdc.202400780.
- 625 **18.** S. Vittorio, F. Lunghini, P. Morerio, D. Gadioli, S. Orlandini, P. Silva, et al., Addressing
626 docking pose selection with structure-based deep learning: recent advances, challenges and
627 opportunities, *Comput. Struct. Biotechnol. J.*, **2024**, *23*, 2141–2151, DOI:
628 10.1016/j.csbj.2024.05.024.
- 629 **19.** F. Rivero-Pino, T. Gonzalez-de la Rosa, M. Torrecillas-Lopez, L. Barrera-Chamorro, J. L.
630 del Rio-Vazquez, E. Marquez-Paradas, et al., Characterization of *Rugulopteryx okamurae* algae:

View Article Online
DOI: 10.1039/D6FO00279J



- 631 a source of bioactive peptides, omega-3 fatty acids, and volatile compounds, *Food Chem.*, **2025**,
632 473, 143084, DOI: 10.1016/j.foodchem.2025.143084. Open Access Article Online
DOI: 10.1039/D6FO00279J
- 633 20. M. Torrecillas-Lopez, C. M. Claro-Cala, T. Gonzalez-de la Rosa, L. Barrera-Chamorro, M.
634 C. Millan-Linares, E. Marquez-Paradas, A. Villanueva, J. L. Del Rio-Vazquez, S. Montserrat-de
635 la Paz, Neuroavailable peptides from hempseed protein hydrolysates reduce hippocampal
636 inflammation and glial activation in a scopolamine-induced Alzheimer's disease model, *Biomed.*
637 *Pharmacother.*, **2025**, *191*, 118438, DOI: 10.1016/j.biopha.2025.118438.
- 638 21. Z. Mai, W. Wei, H. Yu, Y. Chen, Y. Wang, Y. Ding, Molecular recognition of the interaction
639 between ApoE and the TREM2 protein, *Transl. Neurosci.*, **2022**, *13*, 93–103, DOI:
640 10.1515/tnsci-2022-0218.
- 641 22. J. Wen, S. K. Satyanarayanan, A. Li, L. Yan, Z. Zhao, Q. Yuan, et al., Unraveling the impact
642 of omega-3 polyunsaturated fatty acids on blood–brain barrier integrity and glymphatic
643 function, *Brain Behav. Immun.*, **2024**, *115*, 335–355, DOI: 10.1016/j.bbi.2023.10.018.
- 644 23. S. Lopez, B. Bermudez, S. Montserrat-de la Paz, S. Jaramillo, L. M. Varela, A. Ortega-
645 Gomez, R. Abia, F. J. G. Muriana, Membrane composition and dynamics: a target of bioactive
646 virgin olive oil constituents, *Biochim. Biophys. Acta, Biomembr.*, **2014**, *1838*, 1638–1656, DOI:
647 10.1016/j.bbamem.2014.01.007.
- 648 24. M. Slayo, C. Rummel, P. H. Singhaarachchi, M. Feldotto, S. J. Spencer, G. M. Pasinetti, et
649 al., The role of n-3-derived specialised pro-resolving mediators (SPMs) in microglial
650 mitochondrial respiration and inflammation resolution in Alzheimer's disease, *Mol.*
651 *Neurodegener.*, **2025**, *20*, 35, DOI: 10.1186/s13024-025-00824-1.
- 652 25. M. Poxleitner, S. H. L. Hoffmann, G. Berezhnoy, T. M. Ionescu, I. González-Méndez, F. C.
653 Maier, et al., Western diet increases brain metabolism and adaptive immune responses in a
654 mouse model of amyloidosis, *J. Neuroinflammation*, **2024**, *21*, 129, DOI: 10.1186/s12974-024-
655 03080-0.
- 656 26. A. Jagielska, K. Sałaciak, K. Pytka, Beyond the blur: scopolamine's utility and limits in
657 modeling cognitive disorders across sexes—narrative review, *Ageing Res. Rev.*, **2025**, *104*,
658 102635, DOI: 10.1016/j.arr.2024.102635
- 659 27. A. S. Warden, C. Han, E. Hansen, S. Trescott, C. Nguyen, R. Kim, et al., Tools for studying
660 human microglia: in vitro and in vivo strategies, *Brain Behav. Immun.*, **2023**, *107*, 369–382,
661 DOI: 10.1016/j.bbi.2022.10.008.



- 662 28. F. Ren, Y. Luo, P. Liu, H. Xiong, X. Liu, J. Wang, The role of TNF signaling pathway in
663 post-stroke cognitive impairment: a systematic review, *Ann. Med.*, **2025**, *57*, 2543519, DOI:
664 10.1080/07853890.2025.2543519.
- 665 29. H. Ni, Z. Guo, Y. Wu, J. Wang, Y. Yang, Z. Zhu, D. Wang, The crucial role that hippocampus
666 cyclooxygenase-2 plays in memory, *Eur. J. Neurosci.*, **2023**, *58*, 4123–4136, DOI:
667 **10.1111/ejn.16165**.
- 668 30. C.-H. Hsu, Y.-Y. Hsu, B.-M. Chang, K. Raffensperger, M. Kadden, H. T. Ton, et al., StainAI:
669 quantitative mapping of stained microglia and insights into brain-wide neuroinflammation and
670 therapeutic effects in cardiac arrest, *Commun. Biol.*, **2025**, *8*, 462, DOI: 10.1038/s42003-025-
671 07926-y.
- 672 31. T. Hu, C.-H. Liu, M. Lei, Q. Zeng, L. Li, H. Tang, et al., Metabolic regulation of the
673 immune system in health and diseases: mechanisms and interventions *Signal Transduct. Target.*
674 *Ther.*, **2024**, *9*, 268, DOI: 10.1038/s41392-024-01954-6.
- 675 32. M. Cerasuolo, I. Di Meo, M. C. Auriemma, G. Paolisso, M. Papa, M. R. Rizzo, Exploring
676 the dynamic changes of brain lipids, lipid rafts, and lipid droplets in aging and Alzheimer's
677 disease, *Biomolecules*, **2024**, *14*, 1362, DOI: 10.3390/biom14111362
- 678 33. T. Hu, C.-H. Liu, M. Lei, Q. Zeng, L. Li, H. Tang, et al., Metabolic regulation of the
679 immune system in health and diseases: mechanisms and interventions, *Signal Transduct. Target.*
680 *Ther.*, **2024**, *9*, 268, DOI: 10.1038/s41392-024-01954-6.
- 681 34. M. L. Longarzo, A. d'Ambrosio, R. Di Salle, C. Tedeschi, G. Esposito, F. Sorrentino, et al.,
682 Understanding the effects of omega-3 fatty acid supplementation on brain membrane
683 organization, *Prog. Neuropsychopharmacol. Biol. Psychiatry*, **2024**, *127*, 110530, DOI:
684 10.1016/j.pnpbp.2024.110530.
- 685 35. H. Wang, Y. Liu, K. Zhao, P. Li, J. Xu, W. Li, et al., Connexin43 and its regulation of
686 astrocyte gap junction coupling: implications for CNS disease, *Front. Cell Dev. Biol.*, **2025**, *13*,
687 1543981, DOI: 10.3389/fcell.2025.1543981
- 688 36. J.-P. Schuchardt, C. M. Hahn, U. Hahn, A. Hahn, Omega-3 supplementation changes the
689 physical properties of immune-cell membranes, *Prostaglandins Leukot. Essent. Fatty Acids*,
690 **2024**, *198*, 102686, DOI: 10.1016/j.plefa.2024.102686.
- 691 37. L. Wei, H. Zhang, C. Li, Y. Sun, F. Chen, Q. Liu, et al., Neuroprotective properties of extra-
692 virgin olive oil polyphenols: mechanisms and translational outlook, *Nutrients*, **2025**, *17*, 3987,
693 DOI: 10.3390/nu17113987.



- 694 **38.** N. Himaja, J. Niveditha, L. Hu, P. K. Deb, Q. Liu, X. Xue, et al., Development of the
695 "hidden" multi-target-directed ligands by AChE/BuChE for the treatment of Alzheimer's
696 disease, *Eur. J. Med. Chem.*, **2023**, *251*, 115253, DOI:10.1016/j.ejmech.2023.115253.
- 697 **39.** Y. Wan, S. Guan, M. Qian, H. Huang, F. Han, S. Wang, et al., Structural basis of fullerene
698 derivatives as novel potent inhibitors of protein acetylcholinesterase without catalytic active site
699 interaction: insight into the inhibitory mechanism through molecular modeling studies, *J.*
700 *Biomol. Struct. Dyn.*, **2020**, *38*, 410–425, DOI:10.1080/07391102.2019.1576543.
- 701 **40.** K. L. C. Monteiro, M. G. S. Alcântara, N. M. L. Freire, E. M. Brandão, V. L. do
702 Nascimento, L. M. D. S. Viana, et al., BACE-1 Inhibitors Targeting Alzheimer's Disease, *Curr.*
703 *Alzheimer Res.*, **2023**, *20*, 131–148, DOI:10.2174/1567205020666230612155953.
- 704 **41.** A. K. Ghosh, J. Tang, Discovery of Cyclic Sulfone Hydroxyethylamines as Potent and
705 Selective β -Site APP-Cleaving Enzyme 1 (BACE1) Inhibitors: Structure-Based Design and in
706 Vivo Reduction of Amyloid β -Peptides, *J. Med. Chem.*, **2012**, *55*, 9425–9441,
707 DOI:10.1021/jm300069y.
- 708 **42.** J. R. Kiefer, J. L. Pawlitz, K. T. Moreland, R. A. Stegeman, W. F. Hood, J. K. Gierse, et al.,
709 Structural insights into the stereochemistry of the cyclooxygenase reaction, *Nature*, **2000**, *405*,
710 97–101, DOI:10.1038/35011103.
- 711 **43.** M. Shah, R. Parmar, K. Patel, A. Nagani, Indole-based COX-2 inhibitors: A decade of
712 advances in inflammation, cancer, and Alzheimer's therapy, *Bioorg. Chem.*, **2024**, *153*, 107931,
713 DOI:10.1016/j.bioorg.2024.107931.

View Article Online
DOI: 10.1039/D6FO00279J



The data supporting this article have been included as part of the Supplementary Information

[View Article Online](#)
DOI: 10.1039/D6FO00279J

Open Access Article. Published on 17 April 2026. Downloaded on 5/9/2026 1:07:53 PM.
This article is licensed under a Creative Commons Attribution-NonCommercial 3.0 Unported Licence.

